Protein dynamical transition at 110 K

Chae Un Kim[a,1], Mark W. Tate[b,c], and Sol M. Gruner[a,b,c]

[a]Cornell High Energy Synchrotron Source, [b]Laboratory of Atomic and Solid State Physics, and [c]Department of Physics, Cornell University, Ithaca, NY 14853

Edited by William A. Eaton, National Institutes of Health, National Institute of Diabetes and Digestive and Kidney Diseases, Bethesda, MD, and approved November 2, 2011 (received for review July 18, 2011)

Proteins are known to undergo a dynamical transition at around 200 K but the underlying mechanism, physical origin, and relationship to water are controversial. Here we report an observation of a protein dynamical transition as low as 110 K. This unexpected protein dynamical transition precisely correlated with the cryogenic phase transition of water from a high-density amorphous to a low-density amorphous state. The results suggest that the cryogenic protein dynamical transition might be directly related to the two liquid forms of water proposed at cryogenic temperatures.

conformation fluctuations | water phase transition | high-pressure cryocooling | X-ray crystallography

It is known that a hydrated protein undergoes a dynamical transition at around 200 K (1). Proteins below the transition temperature are in a glassy state with little conformational flexibility and no appreciable biological function; above the transition temperature flexibility is restored and the protein becomes biologically active (2–4). This protein dynamical transition has been extensively studied by measuring the mean square atomic displacement, $\langle x^2 \rangle$, of protein atoms as a function of temperature with various methods, including Mössbauer and terahertz time domain spectroscopies (5–7), X-ray crystallography (4, 8–11), neutron scattering (2, 12–19), and molecular dynamics simulations (20–25).

It is believed that the protein dynamical transition involves a strong coupling to the hydration water (10, 26, 27), as a protein dehydrated below a critical level (water/protein mass ratio of ~0.2) does not show the dynamical transition (13, 14, 28). Several mechanisms have been proposed to explain the microscopic origin of protein dynamical transition, including α and β fluctuations in the bulk solvent and the hydration shell (29, 30), liquid-glass transition of hydration water (31), a frequency window scenario (32, 33), and a fragile to strong transition of the hydration water (15, 20).

In this work, we studied a protein dynamical transition inside protein crystals using a high-pressure cryocooling method (34) and temperature-dependent X-ray diffraction (8, 35, 36). Protein crystals contain large amounts of water in solvent channels between the proteins in the crystal lattice; water fractions of greater than 50% are very common. It has been reported that this intracrystalline water can be cryocooled under high pressure into a high-density amorphous (HDA) state that subsequently transforms upon heating to the low-density amorphous (LDA) (36) water typical of ambient-pressure flash-cooling [in bulk water the respective densities of HDA and LDA are 1.17 and 0.94 g cm^{-3} at 77 K and 0.1 MPa. (37, 38)]. In this study, the temperature of the HDA–LDA transition was adjusted by controlling solvent conditions inside the protein crystals. X-ray diffraction data from five thaumatin crystals were used for this study, including four high-pressure cryocooled crystals (Thau-0M-1, Thau-0M-2, Thau-0.45M, Thau-0.9M; 0.9M indicates water solvent that was 0.9 M salt) and one ambient-pressure cryocooled crystal (Thau-control). Details can be found in *Materials and Methods* and *SI Appendix*.

Results

Fig. 1*A* shows the X-ray diffraction images from Thau-0M-1 at four different temperatures from 80 to 160 K. The diffraction image at each temperature provides two independent types of information: The crystal Bragg diffraction provides information on crystal unit-cell parameters, crystal mosaicity (a measure of crystal lattice disorder), protein structure, and the atomic temperature Debye–Waller factor (B-factor) of the protein. The superimposed diffuse diffraction provides the information on the state of the water in the roughly 2- to 4-nm wide solvent channels of the protein crystals.

The crystal Bragg diffraction spots can be filtered out of the diffraction images to extract the water diffuse diffraction (WDD) profiles (see *Materials and Methods*); a shift in the WDD primary peak position is then an indicator of the water phase transition. Fig. 1*B* shows the relative changes in WDD peak positions for four high-pressure cryocooled crystals and one ambient-pressure cryocooled crystal as they were warmed from 80 to 160 K. The phase boundary, defined as the midpoint of the WDD shift moves to higher temperatures (from 125 to 145 K) as the added salt concentration increases in the high-pressure cryocooled crystals. No phase transition was observed with the ambient-pressure cryocooled crystal (Thau-control), which started out in the LDA state at low temperature.

The dynamical transition of the thaumatin molecules was studied by solving protein structures from the Bragg diffraction and monitoring the B-factors of the atomic structures from 80 to 160 K. A B-factor profile purely reflecting harmonic vibrational motions of atoms in a protein differs from one that includes the onset of the molecular fluctuations between different conformational states (8). At very low temperatures conformational freedom in the protein is frozen out and only local vibrational motions are allowed because conformational fluctuations involve activation over energy barriers. In this temperature regime, the B-factor increases almost linearly. As temperature increases, conformational fluctuations become enabled, depending on the height of the activation barrier relevant to the conformational states of a given residue in the protein. In this higher temperature regime, the B-factor increases more rapidly than in the lower temperature regime. A protein dynamical transition has been identified with a sudden change in the slope of the roughly linear increase of the average protein B-factor with temperature (1, 10), which is suggestive of the onset of the conformational fluctuations (see *SI Appendix*).

Fig. 1*C* shows the B-factor profiles of five cryocooled crystals while they were warmed from 80 to 160 K. The B-factor profiles of high-pressure cryocooled crystals (colored curves) clearly show transitions in the temperature range. The breaks from linearity in the B-factor profiles start at roughly 110–120 K for Thau-0M-1 and Thau-0M-2, 135 K for Thau-0.45M, and 140 K for Thau-0.9M. These correlate with the HDA–LDA transition, as seen by changes in the WDD peak positions shown in Fig. 1*B*. By contrast, the ambient-pressure cryocooled crystal (Thau-control;

Author contributions: C.U.K. designed research; C.U.K. performed research; C.U.K. and M.W.T. analyzed data; and C.U.K. and S.M.G. wrote the paper.

The authors declare no conflict of interest.

This article is a PNAS Direct Submission.

[1]To whom correspondence should be addressed. E-mail: ck243@cornell.edu.

This article contains supporting information online at www.pnas.org/lookup/suppl/doi:10.1073/pnas.1110840108/-/DCSupplemental.

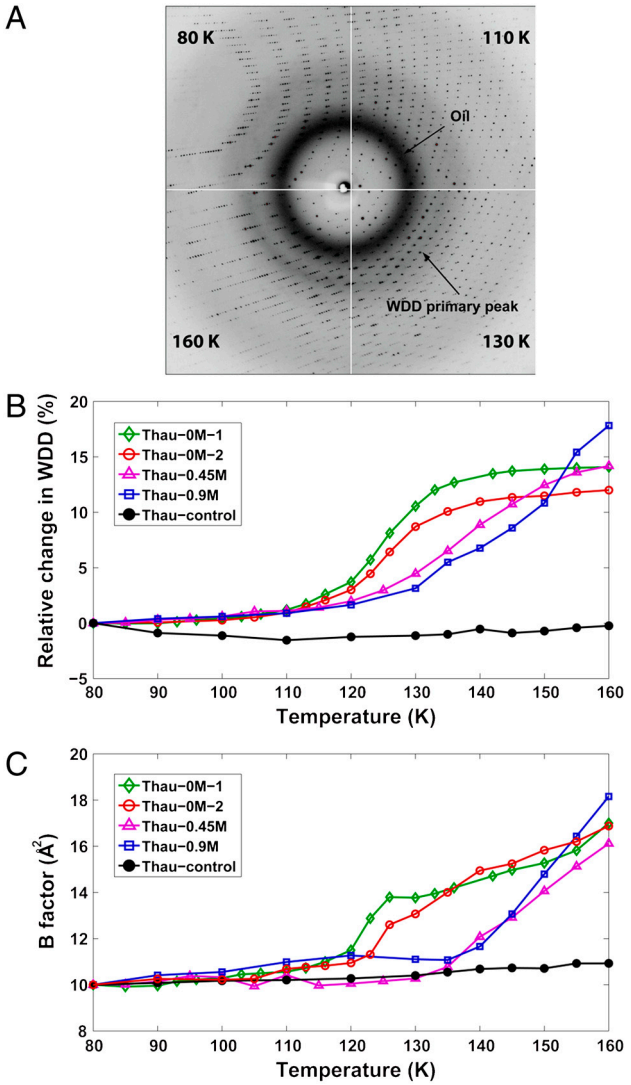

Fig. 1. Protein dynamical transition inside a high-pressure cryocooled crystal. (*A*) X-ray diffraction images of a high-pressure cryocooled crystal (Thau-0M-1) at 80, 110, 130, and 160 K. The diffraction image at each temperature is a superposition of the protein crystallographic Bragg diffraction, diffuse scattering from oil coating the crystals, and WDD. The peak position of WDD shifts as temperature increases, indicating a transition from HDA to LDA states of water. Above 160 K, LDA water turns into cubic ice, leading to protein crystal disruption. (*B*) WDD primary peak position profiles of Thau-0M-1, Thau-0M-2, Thau-0.45M, Thau-0.9M, and Thau-control. Thau-0M-1 and Thau-0M-2 undergo a water transition mostly from 110 to 135 K. Thau-0.45M and Thau-0.9M show rather gradual transition up to higher temperatures. In contrast, Thau-control (black curve) shows little change, indicating no water transition is involved. The WDD primary peak positions can be found in tables in *SI Appendix*. (*C*) Average B-factor profiles (calculated from main chain atoms) of cryocooled thaumatin structures as temperature is raised. The profiles from high-pressure cryocooled crystals (Thau-0M-1, Thau-0M-2, Thau-0.45M, and Thau-0.9M) show changes from linearity indicative of a protein dynamical transition. For each solvent concentration, the temperature for the onset of this behavior roughly correlates with the shift of the WDD shown in Fig. 1*B*. By contrast, the B-factor profile of Thau-control shows no significant transition. The correlation between the WDD peak position profiles and the B-factor profiles suggests that the protein dynamical transition is related to the water phase transition inside the protein crystals. Note that the B-factor profiles are normalized to be 10 at 80 K for comparison (*SI Appendix*). The B-factor values can be found in tables in *SI Appendix*.

Fig. 1*C*, black curve) shows no such transition in the B-factor profile over the range from 80 to 160 K. This observation correlates with no change in the WDD (Fig. 1*B*, black curve), which starts and remains in the LDA state over the given temperature range. These observations suggest that protein structural fluctuations between different conformational states are enabled when the solvent undergoes an HDA–LDA transition and are suppressed if the solvent is in an LDA state throughout (*SI Appendix*).

Although the B-factor analysis discussed above is a useful guideline for a protein dynamical transition, care should be taken in the interpretation of B-factor profiles. The X-ray crystallographic B-factor reflects the mean square atomic displacement $\langle x^2 \rangle$ of atoms in a protein and consists of three dominant terms (8, 10) (*SI Appendix*). The first term accounts for lattice defects in crystalline packing (crystal lattice disorder) and can be monitored by crystal mosaicity. The other terms come from the internal structural motions of protein, which include both harmonic vibrations of individual atoms at a fixed position and molecular fluctuations between different conformational states. The lattice disorder in a protein crystal typically remains unchanged at cryogenic temperatures between 80 and 160 K for crystals that are cryocooled at ambient pressure. However, the lattice disorder in a high-pressure cryocooled protein crystal is changing at cryogenic temperatures through rearrangement in molecular packing (35) (*SI Appendix*). In those regions where the mosaicity is constant (or falling), the faster increase in the B-factor profiles can be attributed to new allowed fluctuations in the conformational states of the protein. However, a full quantitative analysis requires the separation of the lattice disorder term from the B-factor.

To more directly study changes in the protein conformational fluctuations at the HDA–LDA transition we investigated how the structure of the protein changed as temperature rose. The self root-mean-square (self-rms) deviation (see *Materials and Methods*) between the structure at the lowest temperature and the structures at higher temperatures from a single crystal was used as an additional metric for protein dynamical transitions. When previously prohibited structural fluctuations between different conformational states become allowed, one expects the averaged crystallographic structure to become slightly different from the structure before the protein dynamical transition. This structural change would then be reflected in an increase in the self-rms deviation profile.

The self-rms deviation profiles of five cryocooled crystals are plotted in Fig. 2 along with the WDD peak position profiles and B-factor profiles. It is obvious that the self-rms deviation profiles of all four high-pressure cryocooled crystals (Fig. 2 *A*–*D*) are highly correlated with the water phase transition indicated by the WDD peak position profiles. The B-factor profiles show some deviation from the WDD profiles. This deviation is due to the changes in the lattice disorder via molecular rearrangement during crystal warming (*SI Appendix*). The correlation between the self-rms deviation and the WDD peak position profiles suggests that the protein dynamical fluctuations were gradually turned on and the averaged protein structure was evolving in response to the water phase transition. By contrast, the self-rms deviation profile of the ambient-pressure cryocooled crystal (Fig. 2*E*) shows little change, along with no water phase transition over the temperature range. Therefore, we conclude that the observed protein dynamical transition inside a high-pressure cryocooled protein crystal is allowed by the water phase transition inside the crystal.

Discussion

We have presented evidence that thaumatin protein undergoes a dynamical transition as low as 110 K, which is significantly lower than the typically accepted temperature range for the transition (180 ~ 240 K). It has been reported that some proteins exhibit a rapid increase in the mean square atomic displacement below 150 K, but it was attributed to the onset of local structural motions (such as rotational motions of methyl group) rather than the global protein molecular motions (14, 16, 28, 39). Fig. 3*A* shows the averaged B-factor values along the main chain of a high-

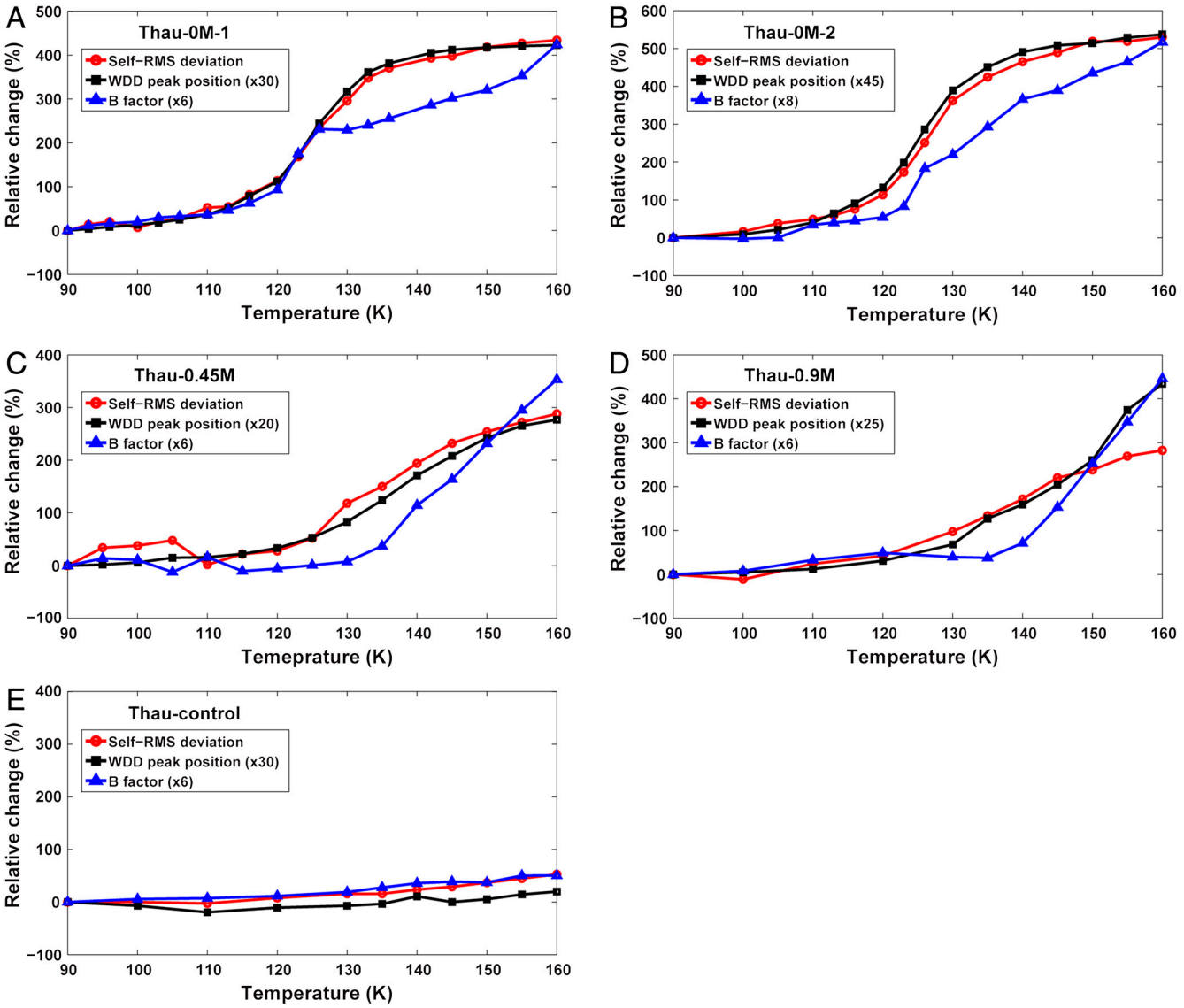

Fig. 2. Self-rms deviation profiles of cryocooled thaumatin structures as an alternative indicator for the protein dynamical transition. The self-rms deviation of each crystal was calculated between the structure at 80 K and the structures at higher temperatures. Plotted is the relative change from the self-rms value at 90 K (see tables in *SI Appendix*). The WDD primary peak position and B-factor profiles (scaled for comparison with self-rms deviation profiles) are superimposed to clarify the correlation between the water transition and the protein dynamical transition. (*A–D*) Self-rms deviation profiles of high-pressure cryocooled crystals (Thau-0M-1, Thau-0M-2, Thau-0.45M, and Thau-0.9M). The self-rms deviation profiles of high-pressure cryocooled crystals show high correlation with the WDD peak position profiles. The B-factor profiles show significant correlation but are less precise, which is due to changes in the crystalline lattice disorder (see main text and *SI Appendix*). (*E*) Self-rms deviation profile of ambient-pressure cryocooled crystal (Thau-control). The profile of Thau-control shows no features of a dynamical transition.

pressure cryocooled thaumatin, Thau-0M-1. As the temperature is raised the B-factor values rise for the entire protein molecule, suggesting that the observed dynamical transition in this study is not due to the increased local motions of a few specific side chains, but is rather due to the global motions over the whole protein molecule. The structural displacements of Thau-0M-1 between 80 and 160 K are illustrated in Fig. 3*B*. The displacements are small, but well outside of measurement error.

During the protein conformational fluctuations, the water surrounding the protein must accommodate changes in the shape of the protein and movement of at least those protein residues in contact with the water. Indeed, solvent mobility, or the translational dynamics of water, was shown to be the dominant factor in determining protein fluctuations in molecular dynamics simulations (21–23). Some proposed mechanisms for the protein dynamical transition at around 200 K (15, 20, 29–31) relate a protein dynamical transition with dynamical motions in hydration water. The fact that we observe thaumatin protein to undergo a cryogenic dynamical transition as low as 110 K suggests that water around the protein gains increased mobility at the HDA–LDA transition, even though it occurs at a deeply cryogenic temperature. This interpretation is consistent with the previous suggestions that protein conformational fluctuations are mainly restricted by the solvent viscosity rather than the potential energy barriers of the protein even at cryogenic temperatures (40–42).

Interestingly, the glass transition temperature of bulk water has been estimated to be 136 K or higher (43). It was reported that confined water shows a glass transition at even higher temperatures than bulk water (44). The viscosity of water diverges as one approaches the water glass transition temperature; therefore, translational diffusive motions of water molecules are restricted. Considering that a protein dynamical transition is triggered by the increased mobility of water around protein, how can we understand the protein dynamical transition at 110 K, well below the

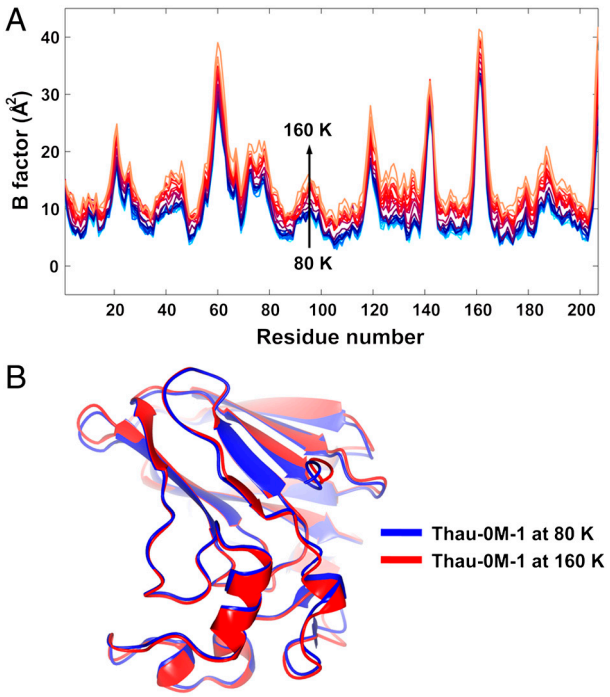

Fig. 3. Global conformational fluctuations during protein dynamical transition. (*A*) The average B-factor values of the main chain atoms along the 207 thaumatin residues. As temperature is raised from 80 to 160 K, the B-factor profiles rise over the whole length of the chain. (*B*) Superposition of the structures of Thau-0M-1 at 80 K (blue) and 160 K (red). The rms atomic displacement in main chain atoms between two structures is 0.235 Å (magnified three times in the figure for visual clarity), which is well above the noise level (~0.05 Å). This result demonstrates that the structural displacements are spread out over the whole protein molecule, indicating that the protein dynamical transition is due to global protein dynamical motions rather than a local motion such as a rotation of methyl group. A site-specific conformational relaxation in the disulfide bond during the dynamical transition can be found in the earlier work (35). Note that the structure at 160 K cannot be generated by the simple rigid-body motions of the structure at 80 K. This observation supports that the rms deviation is not the consequence of the crystal lattice disorder.

known glass transition temperature of water? It is important to note that the cryogenic protein dynamical transition in our study is observed along with the phase transition from HDA to LDA states of water. It has been proposed that the water phase transition from HDA to LDA may involve a high mobility, liquid form of water: The HDA ice first undergoes a glass-liquid transition, then continuously converts to LDA ice (35).

One theoretical explanation for the relationship between the cryogenic protein dynamical transition and the water phase transition from HDA to LDA states can be found from the liquid-liquid (LL) critical point theory (45) for water. The LL critical theory was originally proposed to explain the anomalous thermodynamic properties of the supercooled water (46–48). The theory predicts a first-order phase transition between HDA and LDA ice (35, 46). The theory also requires the liquid state counterparts of HDA and LDA ice (46–48). Based on the LL critical theory, the observed protein dynamical transition at cryogenic temperatures might be related to the two proposed liquid forms of water (high-density liquid and low-density liquid) existing well below the homogeneous nucleation temperature of water (35, 46–49). It remains to be seen how the cryogenic protein dynamical transition is related to the conventional protein dynamical transition at around 200 K, which is thought to be a precondition for a biologically active state of proteins.

Materials and Methods

Protein Crystallization and Crystal Handling. Lyophilized thaumatin powder from *Thaumatococcus daniell* (catalog no. T7638, Sigma) was used for crystallization without further purification. Crystals were grown at 20 °C by the hanging-drop method with 25 mg/mL thaumatin solution in 50 mM Hepes buffer at pH 7 and crystallization solution containing 0.9 M sodium potassium tartrate (NaK tartrate) as a precipitant. The crystal space group was determined to be $P4_12_12$ ($a = b = \sim 58$ Å, $c = \sim 150$ Å), having a solvent content of 60% by volume. To adjust solvent concentrations in protein crystals, the fully grown thaumatin crystals were equilibrated to 0.9 M, 0.45 M sodium potassium tartrate solutions (labeled as Thau-0.9M and Thau-0.45M, respectively), and to deionized water (labeled as Thau-0M-1 and Thau-0M-2), before high-pressure cryocooling at 200 MPa (34). To reduce osmotic shock, crystals were gradually transferred to the target concentration in 0.1 M steps. We found that thaumatin crystals are stable in deionized water over several hours.

Crystal Cryocooling. High-pressure cryocooling of crystal samples was carried out as described by Kim et al. (34). In brief, samples were loaded into the high-pressure cryocooling apparatus, which was then pressurized with helium gas to 200 MPa at ambient temperature. Once at high pressure, the samples were cryocooled to liquid-nitrogen temperature (77 K). Helium pressure was then released. Thereafter crystal samples were handled/stored at ambient pressure and at liquid-nitrogen temperature before X-ray diffraction measurements. For crystals cryocooled at ambient pressure, 20% glycerol (vol/vol) was added to the crystal as a cryoprotectant to reduce crystal damage upon cryocooling. Then the crystal was cryocooled by directly plunging into liquid nitrogen at ambient pressure. An X-ray diffraction study confirmed that the added glycerol does not affect the protein dynamical transition at cryogenic temperatures (*SI Appendix*). Before cryocooling of crystals, liquid surrounding the crystals was carefully removed during crystal-coating with a mineral oil (34). Therefore the water diffuse diffraction is almost entirely from the fluid inside the crystal.

X-Ray Diffraction Data Collection. The X-ray diffraction data were collected at the macromolecular crystallography stations F1 ($\lambda = 0.9179$ Å, Area Detector Systems Corporation (ADSC) Quantum 270 CCD detector, beam size of 100 μm), and F2 ($\lambda = 0.9795$ Å, ADSC Quantum 210 CCD detector, beam size of 150 μm) at the Cornell High Energy Synchrotron Source (CHESS). During data collection, the sample temperature ranging from 80 to 160 K was controlled by a Cryostream 700 series cryocooler (Oxford Cryosystems). The sample temperature was raised at the rate of 6 K/min. After reaching a desired temperature, samples were left at the temperature for 3–5 min for equilibration. The X-ray diffraction data of the protein crystals were collected with temperature steps from 3 to 10 K (see tables in *SI Appendix*). At each temperature, a complete dataset was collected covering 50 to 90° of crystal rotation (50° for Thau-0M-2, 60° for Thau-0.45M/Thau-0.9M/Thau-control, and 90° for Thau-0M-1). The X-ray exposure time was 1 s with oscillation angle of 1°. The data collection parameters were the same for all the complete datasets from a single crystal except for the crystal temperature adjustment.

Data Analysis on Water Diffuse Diffraction. The underlying diffuse diffraction from the diffraction image was isolated from the Bragg spots by applying a custom polar coordinate median filter to the intensity values of the image (36). The sample to detector distance was calibrated based on the known Bragg peaks of hexagonal ice. To determine the position of the WDD peak, the median-filtered diffuse scattering curves were fit to a series of three Voigt functions plus linear background; one Voigt function at the position of the oil scattering peak, one at the main WDD peak, and a third function at the secondary WDD peak.

Structure Refinement. The complete thaumatin datasets were processed and refined with HKL2000 (50) and CCP4 program suite (51). To minimize errors in structural refinement, the structure at 80 K was used as a starting model for the structural refinement at higher temperatures. The refined structures were proofread with COOT (52) and structural errors were carefully corrected. The B-factor values of main chain atoms in the final refined structures were calculated with CCP4 program suite (51). The self-rms deviation between structures at 80 K and higher temperatures were calculated using CCP4 program suite by aligning main chain atoms from residues 1–204 of thaumatin molecules. The final three residues (205–207) were excluded in the self-rms deviation calculation because those residues were highly disordered in all temperatures. Details in data processing and structure refinement can be found in tables in *SI Appendix*.

ACKNOWLEDGMENTS. We thank Marian Szebenyi and Dave Schuller for useful comments, Ji-Won Park for assistance in manuscript preparation, and the Cornell High Energy Synchrotron Source (CHESS) staff for support in data collection. This work is based upon research conducted at CHESS, which is supported by the National Science Foundation (NSF) and the National Institutes of Health (NIH)/National Institute of General Medical Sciences under NSF award DMR-0936384, using the Macromolecular Diffraction at CHESS (MacCHESS) facility, which is supported by award RR-01646 from NIH, through its National Center for Research Resources.

1. Ringe D, Petsko GA (2003) The 'glass transition' in protein dynamics: What it is, why it occurs, and how to exploit it. *Biophys Chem* 105:667–680.
2. Ferrand M, Dianoux AJ, Petry W, Zaccai G (1993) Thermal motions and function of bacteriorhodopsin in purple membranes: Effects of temperature and hydration studied by neutron scattering. *Proc Natl Acad Sci USA* 90:9668–9672.
3. Ostermann A, Waschipky R, Parak FG, Nienhaus GU (2000) Ligand binding and conformational motions in myoglobin. *Nature* 404:205–208.
4. Rasmussen BF, Stock AM, Ringe D, Petsko GA (1992) Crystalline ribonuclease A loses function below the dynamic transition at 220 K. *Nature* 357:423–424.
5. Knapp EW, Fischer SF, Parak F (1982) Protein dynamics from mossbauer spectra. The temperature dependence. *J Phys Chem* 86:5042–5047.
6. He Y, Ku PI, Knab JR, Chen JY, Markelz AG (2008) Protein dynamical transition does not require protein structure. *Phys Rev Lett* 101:178103.
7. Chong SH, et al. (2001) Dynamical transition of myoglobin in a crystal: Comparative studies of X-ray crystallography and Mössbauer spectroscopy. *Eur Biophys J* 30:319–329.
8. Frauenfelder H, Petsko GA, Tsernoglou D (1979) Temperature-dependent X-ray diffraction as a probe of protein structural dynamics. *Nature* 280:558–563.
9. Tilton RF, Dewan JC, Petsko GA (1992) Effects of temperature on protein structure and dynamics: X-ray crystallographic studies of the protein ribonuclease-A at 9 different temperatures from 98 to 320 K. *Biochemistry* 31:2469–2481.
10. Ringe D, Petsko GA (1986) Study of protein dynamics by X-ray diffraction. *Methods Enzymol* 131:389–433.
11. Hartmann H, et al. (1982) Conformational substates in a protein: Structure and dynamics of metmyoglobin at 80 K. *Proc Natl Acad Sci USA* 79:4967–4971.
12. Doster W, Cusack S, Petry W (1989) Dynamical transition of myoglobin revealed by inelastic neutron scattering. *Nature* 337:754–756.
13. Nakagawa H, Joti Y, Kitao A, Kataoka M (2008) Hydration affects both harmonic and anharmonic nature of protein dynamics. *Biophys J* 95:2916–2923.
14. Roh JH, et al. (2005) Onsets of anharmonicity in protein dynamics. *Phys Rev Lett* 95:038101.
15. Chen SH, et al. (2006) Observation of fragile-to-strong dynamic crossover in protein hydration water. *Proc Natl Acad Sci USA* 103:9012–9016.
16. Schiro G, Caronna C, Natali F, Cupane A (2010) Molecular origin and hydration dependence of protein anharmonicity: An elastic neutron scattering study. *Phys Chem Chem Phys* 12:10215–10220.
17. Doster W, et al. (2010) Dynamical transition of protein hydration water. *Phys Rev Lett* 104:098101.
18. Wood K, et al. (2007) Coupling of protein and hydration-water dynamics in biological membranes. *Proc Natl Acad Sci USA* 104:18049–18054.
19. Chu XQ, et al. (2009) Proteins remain soft at lower temperatures under pressure. *J Phys Chem B* 113:5001–5006.
20. Kumar P, et al. (2006) Glass transition in biomolecules and the liquid-liquid critical point of water. *Phys Rev Lett* 97:177802.
21. Tarek M, Tobias DJ (2002) Role of protein-water hydrogen bond dynamics in the protein dynamical transition. *Phys Rev Lett* 88:138101.
22. Tournier AL, Xu JC, Smith JC (2003) Translational hydration water dynamics drives the protein glass transition. *Biophys J* 85:1871–1875.
23. Vitkup D, Ringe D, Petsko GA, Karplus M (2000) Solvent mobility and the protein 'glass' transition. *Nat Struct Biol* 7:34–38.
24. Guo JG, Budarz T, Ward JM, Prohofsky EW (2010) Dynamical transition in proteins and non-Gaussian behavior of low-frequency modes in self-consistent normal mode analysis. *Phys Rev E* 82:041917.
25. Kohn JE, Afonine PV, Ruscio JZ, Adams PD, Head-Gordon T (2010) Evidence of functional protein dynamics from X-ray crystallographic ensembles. *PLoS Comput Biol* 6:e1000911.
26. Fenimore PW, Frauenfelder H, McMahon BH, Parak FG (2002) Slaving: Solvent fluctuations dominate protein dynamics and functions. *Proc Natl Acad Sci USA* 99:16047–16051.
27. Teeter MM, Yamano A, Stec B, Mohanty U (2001) On the nature of a glassy state of matter in a hydrated protein: Relation to protein function. *Proc Natl Acad Sci USA* 98:11242–11247.
28. Roh JH, et al. (2006) Influence of hydration on the dynamics of lysozyme. *Biophys J* 91:2573–2588.
29. Frauenfelder H, et al. (2009) A unified model of protein dynamics. *Proc Natl Acad Sci USA* 106:5129–5134.
30. Fenimore PW, Frauenfelder H, McMahon BH, Young RD (2004) Bulk-solvent and hydration-shell fluctuations, similar to alpha- and beta-fluctuations in glasses, control protein motions and functions. *Proc Natl Acad Sci USA* 101:14408–14413.
31. Doster W (2010) The protein-solvent glass transition. *Biochim Biophys Acta* 1804:3–14.
32. Becker T, Hayward JA, Finney JL, Daniel RM, Smith JC (2004) Neutron frequency windows and the protein dynamical transition. *Biophys J* 87:1436–1444.
33. Khodadadi S, et al. (2008) The origin of the dynamic transition in proteins. *J Chem Phys* 128:195106.
34. Kim CU, Kapfer R, Gruner SM (2005) High pressure cooling of protein crystals without cryoprotectants. *Acta Crystallogr Sect D Biol Crystallogr* 61:881–890.
35. Kim CU, Barstow B, Tate MW, Gruner SM (2009) Evidence for liquid water during the high-density to low-density amorphous ice transition. *Proc Natl Acad Sci USA* 106:4596–4600.
36. Kim CU, Chen YF, Tate MW, Gruner SM (2008) Pressure induced high-density amorphous ice in protein crystals. *J Appl Crystallogr* 41:1–7.
37. Mishima O, Calvert LD, Whalley E (1984) 'Melting ice' I at 77 K and 10 kbar: A new method of making amorphous solids. *Nature* 310:393–395.
38. Ghormley JA, Hochanad CJ (1971) Amorphous ice—density and reflectivity. *Science* 171:62–64.
39. Lee AL, Wand AJ (2001) Microscopic origins of entropy, heat capacity and the glass transition in proteins. *Nature* 411:501–504.
40. Ansari A, Jones CM, Henry ER, Hofrichter J, Eaton WA (1992) The role of solvent viscosity in the dynamics of protein conformational changes. *Science* 256:1796–1798.
41. Ansari A, Jones CM, Henry ER, Hofrichter J, Eaton WA (1994) Conformational relaxation and ligand binding in myoglobin. *Biochemistry* 33:5128–5145.
42. Hagen SJ, Hofrichter J, Eaton WA (1996) Geminate rebinding and conformational dynamics of myoglobin embedded in a glass at room temperature. *J Phys Chem* 100:12008–12021.
43. Velikov V, Borick S, Angell CA (2001) The glass transition of water, based on hyperquenching experiments. *Science* 294:2335–2338.
44. Cerveny S, Schwartz GA, Bergman R, Swenson J (2004) Glass transition and relaxation processes in supercooled water. *Phys Rev Lett* 93:245702.
45. Poole PH, Sciortino F, Essmann U, Stanley HE (1992) Phase behavior of metastable water. *Nature* 360:324–328.
46. Mishima O, Stanley HE (1998) The relationship between liquid, supercooled and glassy water. *Nature* 396:329–335.
47. Debenedetti PG (2003) Supercooled and glassy water. *J Phys Condens Matter* 15: R1669–R1726.
48. Debenedetti PG, Stanley HE (2003) Supercooled and glassy water. *Phys Today* 56:40–46.
49. Stanley HE, et al. (2007) The puzzling unsolved mysteries of liquid water: Some recent progress. *Physica A* 386:729–743.
50. Otwinowski Z, Minor W (1997) Processing of X-ray diffraction data collected in oscillation mode. *Methods Enzymol* 276:307–326.
51. Collaborative Computational Project No. 4 (1994) The ccp4 suite: Programs for protein crystallography. *Acta Crystallogr Sect D Biol Crystallogr* 50:760–763.
52. Emsley P, Cowtan K (2004) Coot: Model-building tools for molecular graphics. *Acta Crystallogr Sect D Biol Crystallogr* 60:2126–2132.

Supporting Information

Kim et al. 'Protein Dynamical Transition at 110 K'

1. Sample information

In this study, X-ray diffraction data sets from 6 Thaumatin crystals were used (5 crystals for the main text, 1 additional crystal for Supporting Information). Information on each crystal is as follows.

1) **Thau-0M-1**: Equilibrated to de-ionized water, pressure cryocooled at 200 MPa.
2) **Thau-0M-2**: Equilibrated to de-ionized water, pressure cryocooled at 200 MPa.
3) **Thau-0.45M**: Equilibrated to 0.45 M Sodium Potassium tartrate solution, pressure cryocooled at 200 MPa.
4) **Thau-0.9M**: Equilibrated to 0.9 M Sodium Potassium tartrate solution, pressure cryocooled at 200 MPa.
5) **Thau-control**: Equilibrated to 0.9 M Sodium Potassium tartrate solution, cryoprotected with 20 % glycerol (v/v), cryocooled at 0.1 MPa.
6) **Thau-control-noGLY**: Equilibrated to 1.5 M Sodium Potassium tartrate solution, no glycerol added, cryocooled at 0.1 MPa.

X-ray diffraction data collection and refinement statistics for each crystal can be found in Table S1-S12 at the end.

2. Interpretation of the B-factor and the self-RMS deviation profiles

The protein dynamical transition has been studied by monitoring the mean square atomic displacement ($\langle x^2 \rangle$) of protein atoms. In X-ray protein crystallography, the atomic displacement consists of three major terms (1).

$$\langle x^2 \rangle_{total} = \langle x^2 \rangle_{lattice} + \langle x^2 \rangle_{vib} + \langle x^2 \rangle_{conf}$$

The first term ($<x^2>_{lattice}$) is the contribution due to lattice disorder. It is a static disorder and typically does not change at cryogenic temperatures if a protein crystal is cryocooled at ambient pressure. However, it was observed that crystal lattice disorder can be changing during crystal warming when the crystal is cryocooled at high pressure(2). The changes in the crystal lattice disorder can be monitored by crystal mosaicity.

The second term ($<x^2>_{vib}$) is the contribution due to atomic vibrational motions and is linearly increasing when temperature increases both in the high pressure cryocooled and ambient pressure cryocooled protein crystals. The third term ($<x^2>_{conf}$) is the contribution due to the protein conformational fluctuations and reflects either the static distributions of conformational states or the dynamical motions between conformational states. Although the X-ray diffraction measurement cannot distinguish the difference between the static distribution and the dynamical motions, the temperature dependence of the third term provides the clues for the dynamical fluctuations. The nonlinear increase in the third term indicates that protein conformational fluctuations are enabled at least transiently while temperature increases.

In our study, it was observed that the B-factor profiles and the self-RMS deviation profiles from high pressure cryocooled crystals show nonlinear behavior upon warming. The crystal mosaicity profiles of high pressure cryocooled crystals (section 4 in this supporting information) indicate that the crystal lattice disorder is not a major term for the nonlinearity. As lattice disorder and atomic vibrational motions do not account for this nonlinear behavior, we concluded that the experimental results (Fig 1, Fig 2) reflect the gained dynamical fluctuations during the HDA-LDA phase transition. Our interpretation is following.

When a protein molecule is trapped in LDA ice (Thau-control), large conformational fluctuations are frozen out. Therefore, only a small linear increase in the B-factor and self-RMS deviation profiles is observed when temperature increases.

On the other hand, during the HDA to LDA ice transition, protein molecules are possibly exposed to a transient fluid environment, allowing large conformational fluctuations(2). When the transition is completed, further dynamical motions of the protein molecules may be again frozen. But this frozen state represents the final, higher temperature distribution of the conformational states right before being refrozen. This can cause a rapid increase in the B-factor and the self-RMS deviation profiles, showing nonlinearity.

It is important to note that the B-factor and the self-RMS deviation values of a cryocooled protein are not fully determined by the final ice state because there is no guarantee that the state that is frozen is in full thermal equilibrium. The approach to thermal equilibrium may be path dependent. The final conformational states of a protein after the HDA-LDA transition at a given temperature can be different from the states of a protein trapped in the LDA ice. This can explain the observed higher B-factor and self-RMS deviation values for the high-pressure cryocooled protein crystals after HDA-LDA transition (table S1-S12) compared to proteins which were warmed to the same temperature, but have been trapped in LDA ice throughout the warming process.

Note that the absolute B-factor values (table S1-S12) of a protein depend on the initial crystal quality and the way that the protein crystal is handled before X-ray diffraction measurement. Therefore, directly comparing the absolute B factor values between different crystals can be misleading. The protein dynamical transition is detected by the nonlinear changes in the B-factor profiles, which does not require the absolute values. For this reason, the initial B factor values of different thaumatin crystals are normalized to be 10 at 80 K in Fig. 1C in the main article.

3. Changes in crystal lattice disorder during protein dynamical transition

Crystal mosaicity is a measure of disorder in unit-cell alignment and reflects the lattice disorder in a protein crystal. Fig. S1A shows the crystal mosaicity profiles of 4 high pressure cryocooled crystals (Thau-0M-1, Thau-0M-2, Thau-0.45M, and Thau-0.9M) and 1 ambient pressure cryocooled crystal (Thau-control). The mosaicity profiles of high pressure cryocooled crystals show significant fluctuations compared to the profile from

Thau-control. Note that the crystal mosaicity of high-pressure cryocooled crystals show improvement (between 110 K and 140 K for Thau-0M-2/Thau-0.45M/Thau-0.9M, and between 125 K and 142 K for Thau-0M-1), indicating that the crystal lattice disorder actually decreased over the temperature range. This observation supports that the observed nonlinear behaviors in the B-factor profiles and the self-RMS profiles (Figure 1C and Figure 2 in the main text) are the consequence of the protein conformational fluctuations rather than the increased lattice disorder. Fig. S1B shows that the improvement in the crystal mosaicity above 126 K affects the B-factor profile of the high pressure cryocooled crystal, suggesting that the B-factor profile of a high pressure cryocooled crystal not only represents the protein conformational fluctuations but also the changes in the crystal lattice disorder. Note that the B-factor profile still rises above 126 K when the crystal mosaicity improves (i.e. lattice disorder decreases). This indicates that the B-factor profile mainly reflects the protein dynamical fluctuations rather than the crystal lattice disorder.

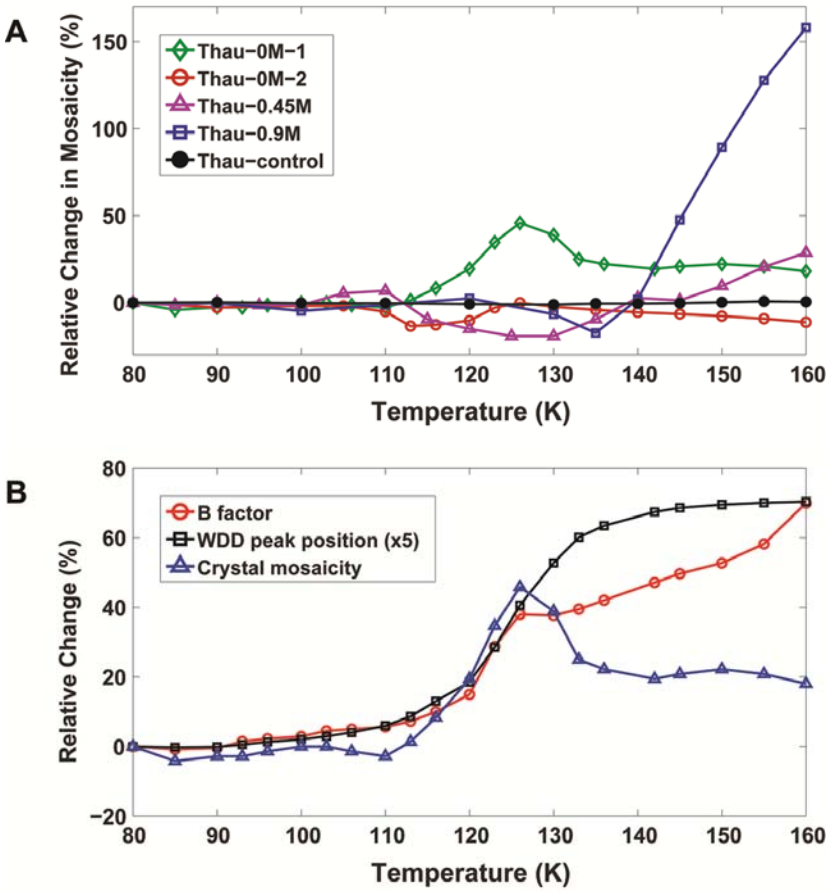

Fig. S1 Crystal mosaicity profiles of cryocooled crystals (Thau-0M-1, Thau-0M-2, Thau-0.45M, Thau-0.9M, and Thau-control) from 80 K to 160 K. (A) The high pressure cryocooled crystals show significant fluctuations in the temperature range, indicating some changes in the crystal lattice disorder via molecular rearrangement. In contrast, the ambient pressure cryocooled crystal (Thau-control) shows little fluctuations. (B) Superposition of crystal mosaicity with B factor and WDD primary peak position profiles of Thau-0M-1. Note that the B factor profile shows some deviation from the WDD peak position profile right above 126 K where the crystal mosaicity begins to fall down.

4. Effects of glycerol on cryogenic protein dynamical transition

The 4 high pressure cryocooled crystals (Thau-0M-1, Thau-0M-2, Thau-0.45M, Thau-0.9M) were cryocooled without adding glycerol. However, high quality X-ray diffraction data sets could be collected because cryocooling of protein crystals under high pressure eliminates the need for chemical cryoprotectants(3). In contrast, the ambient pressure cryocooled crystal (Thau-control) was soaked into 20 % glycerol (v/v) containing solution before cryocooling for crystal cryoprotection. To see the effect of glycerol on the protein dynamical transition at cryogenic temperature, additional Thaumatin crystal (Thau-control-noGLY) was cryocooled at ambient pressure without adding glycerol. The B factor profiles of Thau-control and Thau-control-noGLY in Fig. S2 show no features of protein dynamical transition at cryogenic temperatures, therefore eliminating the possibility that the absence of glycerol in the high pressure cryocooled crystals is the cause for the protein dynamical transition. Note that the X-ray diffraction quality of Thau-control-noGLY as shown in Table S11 is poorer (in terms of crystal mosaicity, R_{sym}, and $I/\sigma(I)$) than Thau-control (Table S9) as a consequence of crystal damage during cryocooling at ambient pressure without chemical cryoprotectants.

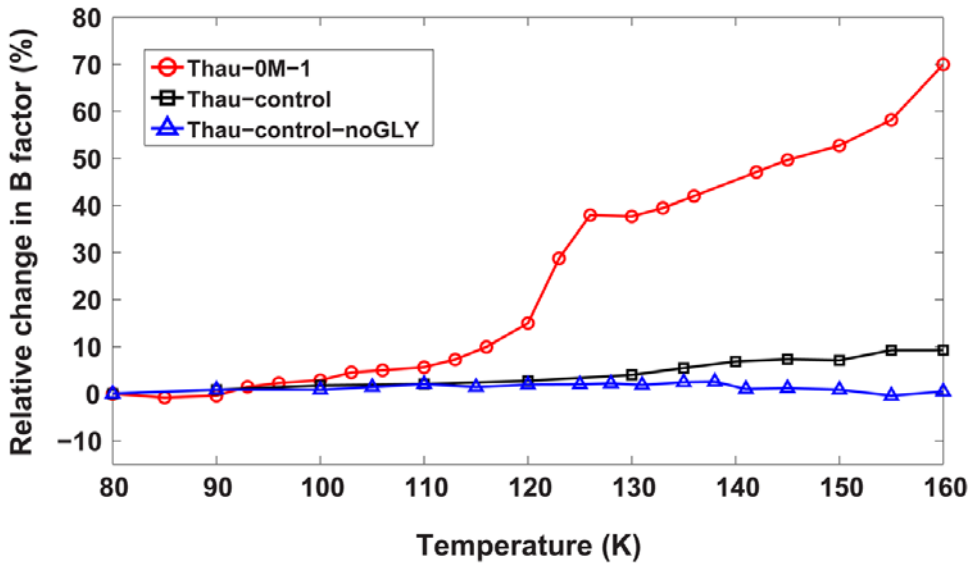

Fig. S2 The B factor profiles of Thau-control and Thau-control-noGLY along with the profile of Thau-0M-1 as a reference. The Thau-0M-1 profile shows nonlinearity above 110 K, indicative of protein dynamical transition. In contrast, no clear nonlinearity is observed from Thau-control and Thau-control-noGLY. This result suggests that the absence of glycerol in the high pressure cryocooled crystal is not responsible for the observed protein dynamical transition.

Reference

1. Ringe D, Petsko GA (1986) Study of protein dynamics by x-ray diffraction. *Methods Enzymol* 131:389-433.
2. Kim CU, Barstow B, Tate MW, Gruner SM (2009) Evidence for liquid water during the high-density to low-density amorphous ice transition. *Proc Natl Acad Sci USA* 106:4596-4600.
3. Kim CU, Kapfer R, Gruner SM (2005) High pressure cooling of protein crystals without cryoprotectants. *Acta Crystallogr D* 61:881-890.

Table S1. Data collection statistics of Thau-0M-1

Temp (K)	Unit-cell dimensions (Å)		Resolution (Å)	Mosaicity (°)	R_{sym} [a]	I/σ(I)	Completeness (%)	Redundancy
	a=b	c						
80	57.36	149.02	30-2.0 (2.03-2.0)	0.360	0.053 (0.081)	36.2 (17.1)	99.4 (99.8)	6.9 (5.6)
85	57.37	149.06	30-2.0 (2.03-2.0)	0.345	0.045 (0.076)	41.4 (18.3)	99.3 (99.8)	6.9 (5.6)
90	57.39	149.11	30-2.0 (2.03-2.0)	0.350	0.049 (0.079)	37.9 (17.4)	99.3 (99.9)	6.9 (5.6)
93	57.41	149.15	30-2.0 (2.03-2.0)	0.350	0.047 (0.078)	40.3 (18.1)	99.3 (99.9)	6.9 (5.6)
96	57.43	149.18	30-2.0 (2.03-2.0)	0.355	0.046 (0.077)	41.1 (18.0)	99.3 (99.9)	6.9 (5.6)
100	57.45	149.24	30-2.0 (2.03-2.0)	0.360	0.046 (0.079)	41.7 (18.3)	99.3 (99.9)	6.9 (5.6)
103	57.47	149.29	30-2.0 (2.03-2.0)	0.360	0.045 (0.077)	41.3 (18.2)	99.3 (99.9)	6.9 (5.6)
106	57.50	149.36	30-2.0 (2.03-2.0)	0.355	0.046 (0.082)	41.7 (17.6)	99.3 (100)	6.9 (5.6)
110	57.54	149.46	30-2.0 (2.03-2.0)	0.350	0.046 (0.082)	41.4 (17.5)	99.3 (99.9)	6.9 (5.6)
113	57.59	149.56	30-2.0 (2.03-2.0)	0.365	0.046 (0.084)	40.1 (16.5)	99.3 (99.9)	6.9 (5.6)
116	57.65	149.68	30-2.0 (2.03-2.0)	0.390	0.047 (0.086)	39.9 (15.6)	99.3 (99.7)	6.9 (5.5)
120	57.74	149.87	30-2.0 (2.03-2.0)	0.430	0.049 (0.098)	39.2 (14.6)	99.2 (99.8)	6.9 (5.7)
123	57.86	150.12	30-2.0 (2.03-2.0)	0.485	0.051 (0.111)	37.1 (12.8)	99.2 (99.9)	6.9 (5.7)
126	58.05	150.41	30-2.0 (2.03-2.0)	0.525	0.053 (0.120)	36.2 (11.3)	99.2 (99.9)	6.9 (5.8)
130	58.26	150.73	30-2.0 (2.03-2.0)	0.500	0.053 (0.119)	34.9 (12.4)	99.1 (98.5)	6.9 (5.9)
133	58.39	150.93	30-2.0 (2.03-2.0)	0.450	0.050 (0.108)	37.6 (13.9)	99.1 (98.4)	7.0 (5.8)
136	58.46	150.98	30-2.0 (2.03-2.0)	0.440	0.050 (0.108)	37.3 (12.9)	99.1 (98.9)	6.9 (5.7)
142	58.56	151.03	30-2.0 (2.03-2.0)	0.430	0.051 (0.111)	37.5 (12.7)	99.1 (99.1)	7.0 (5.7)
145	58.61	151.03	30-2.0 (2.03-2.0)	0.435	0.051 (0.118)	35.8 (11.6)	99.1 (99.4)	7.0 (5.6)
150	58.66	151.03	30-2.0 (2.03-2.0)	0.440	0.052 (0.122)	36.6 (11.6)	99.1 (99.6)	6.9 (5.6)
155	58.72	151.02	30-2.0 (2.03-2.0)	0.435	0.053 (0.129)	36.6 (10.7)	99.1 (99.6)	7.0 (5.6)
160	58.78	151.01	30-2.0 (2.03-2.0)	0.425	0.052 (0.123)	36.9 (11.0)	99.1 (99.6)	6.9 (5.6)

[a] $R_{sym} = \Sigma |I - \langle I \rangle| / \Sigma \langle I \rangle$

Table S2. Refinement statistics of Thau-0M-1

Temp (K)	Unique reflections	R factor [a]	R_{free} factor [b]	B factor (Å^2) – main chain	Self-RMS deviation [c] (Å)	WDD peak position (Å) [d]
80	17513	0.166	0.225	9.24	0	3.26
85	17532	0.167	0.221	9.16	0.046	3.26
90	17549	0.165	0.222	9.20	0.044	3.26
93	17571	0.165	0.217	9.37	0.05	3.27
96	17578	0.170	0.228	9.45	0.053	3.27
100	17598	0.162	0.232	9.50	0.047	3.28
103	17606	0.167	0.240	9.65	0.053	3.28
106	17621	0.164	0.227	9.70	0.056	3.29
110	17659	0.169	0.248	9.76	0.067	3.30
113	17685	0.165	0.243	9.91	0.068	3.32
116	17883	0.166	0.234	10.16	0.080	3.35
120	17789	0.167	0.235	10.62	0.094	3.39
123	17860	0.168	0.231	11.89	0.118	3.45
126	17980	0.168	0.230	12.75	0.147	3.53
130	18118	0.168	0.224	12.72	0.174	3.61
133	18260	0.169	0.224	12.88	0.197	3.66
136	18319	0.167	0.227	13.12	0.207	3.68
142	18384	0.167	0.224	13.59	0.217	3.70
145	18415	0.168	0.219	13.83	0.219	3.71
150	18445	0.169	0.216	14.11	0.228	3.72
155	18494	0.173	0.217	14.61	0.232	3.72
160	18521	0.169	0.214	15.70	0.235	3.72

[a] R factor = Σ $|F_o| - |F_c| / \Sigma |F_{obs}|$

[b] R_{free} factor is calculated the same as R factor, except it uses 5 % of reflection data omitted from refinement

[c] Self-RMS deviation was calculated between the structure at 80 K and the structures at higher temperatures of Thau-0M-1.

[d] WDD peak position in d-spacing: $d = 2\pi/Q$, where the momentum transfer vector Q is given by $Q = 4\pi\sin(\theta)/\lambda$, where λ is the X-ray wavelength and 2θ is the angle between the incident beam and the diffracted X-rays.

Table S3. Data collection statistics of Thau-0M-2

Temp (K)	Unit-cell dimensions (Å)		Resolution (Å)	Mosaicity (°)	R_{sym} [a]	I/σ(I)	Completeness (%)	Redundancy
	a=b	c						
80	57.58	149.94	50-1.8 (1.83-1.8)	0.53	0.047 (0.120)	28.1 (8.2)	96.4 (93.4)	4.0 (3.7)
90	57.59	149.99	50-1.8 (1.83-1.8)	0.515	0.046 (0.119)	28.6 (8.5)	96.4 (93.3)	4.0 (3.7)
100	57.63	150.09	50-1.8 (1.83-1.8)	0.521	0.047 (0.119)	28.7 (8.3)	96.3 (93.2)	4.0 (3.7)
105	57.68	150.18	50-1.8 (1.83-1.8)	0.521	0.046 (0.125)	28.3 (8.2)	96.2 (92.7)	4.0 (3.7)
110	57.74	150.20	50-1.8 (1.83-1.8)	0.503	0.048 (0.126)	28.8 (8.3)	96.1 (92.4)	4.0 (3.7)
113	57.78	150.26	50-1.8 (1.83-1.8)	0.459	0.047 (0.121)	29.3 (8.6)	96.1 (92.3)	4.0 (3.7)
116	57.84	150.38	50-1.8 (1.83-1.8)	0.463	0.048 (0.122)	29.1 (8.4)	96.1 (92.1)	4.0 (3.7)
120	57.93	150.54	50-1.8 (1.83-1.8)	0.476	0.048 (0.126)	28.4 (8.2)	96.0 (92.5)	4.0 (3.7)
123	58.07	150.79	50-1.8 (1.83-1.8)	0.515	0.050 (0.139)	26.4 (7.2)	95.9 (92.5)	4.0 (3.7)
126	58.24	151.08	50-1.8 (1.83-1.8)	0.53	0.053 (0.163)	25.1 (6.0)	95.8 (92.8)	4.0 (3.7)
130	58.47	151.46	50-1.8 (1.83-1.8)	0.518	0.055 (0.171)	24.9 (5.5)	92.4 (93.1)	4.1 (3.7)
135	58.65	151.67	530-1.8 (1.83-1.8)	0.508	0.053 (0.184)	26.4 (5.5)	90.6 (92.1)	4.2 (3.7)
140	58.76	151.74	50-1.8 (1.83-1.8)	0.501	0.053 (0.201)	25.9 (5.2)	89.9 (92.1)	4.3 (3.7)
145	58.84	151.73	50-1.8 (1.83-1.8)	0.496	0.054 (0.208)	26.4 (4.8)	89.6 (91.9)	4.3 (3.7)
150	58.90	151.70	50-1.8 (1.83-1.8)	0.490	0.053 (0.220)	26.1 (4.7)	89.4 (91.7)	4.3 (3.7)
155	58.95	151.66	50-1.8 (1.83-1.8)	0.481	0.054 (0.226)	25.8 (4.2)	89.3 (91.6)	4.3 (3.7)
160	58.99	151.61	50-1.8 (1.83-1.8)	0.471	0.055 (0.247)	25.5 (4.0)	89.2 (91.4)	4.3 (3.8)

[a] $R_{sym} = \Sigma |I - \langle I \rangle| / \Sigma \langle I \rangle$

Table S4. Refinement statistics of Thau-0M-2

Temp (K)	Unique reflections	R factor [a]	R_{free} factor [b]	B factor (Å^2) – main chain	Self-RMS deviation [c] (Å)	WDD peak position (Å) [d]
80	23420	0.159	0.216	8.34	0	3.27
90	23416	0.160	0.216	8.55	0.037	3.27
100	23439	0.162	0.211	8.52	0.043	3.28
105	23484	0.159	0.213	8.55	0.051	3.28
110	23518	0.157	0.203	8.91	0.055	3.30
113	23607	0.159	0.214	8.97	0.059	3.32
116	23676	0.158	0.202	9.02	0.065	3.34
120	23764	0.158	0.216	9.13	0.079	3.37
123	23884	0.154	0.204	9.43	0.101	3.41
126	24023	0.158	0.216	10.51	0.130	3.48
130	23407	0.160	0.209	10.90	0.171	3.55
135	23121	0.157	0.210	11.68	0.194	3.60
140	23021	0.158	0.204	12.46	0.209	3.63
145	23012	0.163	0.216	12.71	0.218	3.64
150	22999	0.163	0.209	13.20	0.229	3.64
155	23004	0.167	0.226	13.51	0.229	3.65
160	22993	0.165	0.219	14.07	0.233	3.66

[a] R factor = $\Sigma\ |F_o| - |F_c| / \Sigma\ |F_{obs}|$

[b] R_{free} factor is calculated the same as R factor, except it uses 5 % of reflection data omitted from refinement

[c] Self-RMS deviation was calculated between the structure at 80 K and the structures at higher temperatures of Thau-0M-2.

[d] WDD peak position in d-spacing: $d = 2\pi/Q$, where the momentum transfer vector Q is given by $Q = 4\pi\sin(\theta)/\lambda$, where λ is the X-ray wavelength and 2θ is the angle between the incident beam and the diffracted X-rays.

Table S5. Data collection statistics of Thau-0.45M

Temp (K)	Unit-cell dimensions (Å)		Resolution (Å)	Mosaicity (°)	R_{sym} [a]	I/σ(I)	Completeness (%)	Redundancy
	a=b	c						
80	57.26	149.39	50-1.9 (1.93-1.9)	0.365	0.051 (0.124)	29.2 (8.8)	98.2 (97.3)	4.7 (4.2)
85	57.27	149.42	50-1.9 (1.93-1.9)	0.36	0.051 (0.123)	28.6 (8.9)	98.2 (97.3)	4.7 (4.3)
90	57.27	149.45	50-1.9 (1.93-1.9)	0.365	0.052 (0.117)	28.2 (9.2)	97.9 (97.4)	4.7 (4.2)
95	57.29	149.49	50-1.9 (1.93-1.9)	0.36	0.048 (0.111)	30.5 (10.0)	98.2 (97.4)	4.7 (4.2)
100	57.31	149.55	50-1.9 (1.93-1.9)	0.36	0.046 (0.113)	31.6 (9.5)	98.1 (97.2)	4.7 (4.2)
105	57.34	149.56	50-1.9 (1.93-1.9)	0.385	0.050 (0.126)	31.4 (9.3)	98.1 (97.5)	4.7 (4.2)
110	57.38	149.63	50-1.9 (1.93-1.9)	0.39	0.047 (0.120)	31.9 (9.4)	98.2 (97.2)	4.7 (4.2)
115	57.42	149.70	50-1.9 (1.93-1.9)	0.33	0.046 (0.115)	31.7 (9.9)	98.3 (97.3)	4.7 (4.3)
120	57.48	149.83	50-1.9 (1.93-1.9)	0.31	0.046 (0.112)	31.7 (10.0)	98.3 (97.4)	4.7 (4.3)
125	57.57	150.03	50-1.9 (1.93-1.9)	0.295	0.045 (0.109)	33.8 (11.0)	98.4 (97.8)	4.7 (4.2)
130	57.69	150.27	50-1.9 (1.93-1.9)	0.295	0.046 (0.112)	34.3 (11.3)	98.4 (97.7)	4.7 (4.3)
135	57.85	150.55	50-1.9 (1.93-1.9)	0.33	0.047 (0.122)	32.3 (10.1)	98.4 (97.8)	4.7 (4.3)
140	58.01	150.82	50-1.9 (1.93-1.9)	0.375	0.050 (0.152)	31.3 (8.1)	98.4 (98.1)	4.7 (4.3)
145	58.18	151.02	50-1.9 (1.93-1.9)	0.37	0.052 (0.161)	30.0 (7.5)	98.5 (99.0)	4.7 (4.2)
150	58.30	151.12	50-1.9 (1.93-1.9)	0.4	0.055 (0.192)	28.8 (6.2)	98.6 (99.1)	4.7 (4.2)
155	58.40	151.15	50-1.9 (1.93-1.9)	0.44	0.058 (0.222)	26.8 (5.3)	98.6 (99.1)	4.7 (4.2)
160	58.48	151.14	50-1.9 (1.93-1.9)	0.47	0.061 (0.229)	25.6 (4.5)	98.6 (99.1)	4.7 (4.2)

[a] $R_{sym} = \Sigma |I - \langle I \rangle| / \Sigma \langle I \rangle$

Table S6. Refinement statistics of Thau-0.45M

Temp (K)	Unique reflections	R factor [a]	R_{free} factor [b]	B factor (Å^2) – main chain	Self-RMS deviation [c] (Å)	WDD peak position (Å) [d]
80	20209	0.162	0.223	9.64	0	3.12
85	20211	0.161	0.216	9.66	0.036	3.12
90	20168	0.162	0.209	9.78	0.050	3.13
95	20229	0.161	0.222	10.01	0.067	3.13
100	20252	0.158	0.222	9.96	0.069	3.14
105	20241	0.160	0.217	9.58	0.074	3.15
110	20283	0.162	0.216	10.05	0.051	3.16
115	20342	0.161	0.224	9.61	0.061	3.17
120	20409	0.162	0.208	9.69	0.064	3.18
125	20516	0.160	0.204	9.80	0.076	3.21
130	20656	0.159	0.209	9.90	0.109	3.26
135	20855	0.161	0.215	10.39	0.125	3.32
140	21028	0.162	0.208	11.64	0.147	3.40
145	21154	0.163	0.212	12.45	0.166	3.46
150	21276	0.164	0.212	13.56	0.177	3.51
155	21345	0.169	0.219	14.59	0.186	3.55
160	21421	0.174	0.215	15.54	0.194	3.56

[a] R factor = $\Sigma\ |F_o| - |F_c| / \Sigma\ |F_{obs}|$

[b] R_{free} factor is calculated the same as R factor, except it uses 5 % of reflection data omitted from refinement

[c] Self-RMS deviation was calculated between the structure at 80 K and the structures at higher temperatures of Thau-0.45M.

[d] WDD peak position in d-spacing: $d = 2\pi/Q$, where the momentum transfer vector Q is given by $Q = 4\pi\sin(\theta)/\lambda$, where λ is the X-ray wavelength and 2θ is the angle between the incident beam and the diffracted X-rays.

Table S7. Data collection statistics of Thau-0.9M

Temp (K)	Unit-cell dimensions (Å)		Resolution (Å)	Mosaicity (°)	R_{sym} [a]	I/σ(I)	Completeness (%)	Redundancy
	a=b	c						
80	57.43	149.90	30-1.9 (1.97-1.9)	0.317	0.029 (0.056)	49.2 (19.4)	98.4 (87.0)	4.4 (3.1)
90	57.46	149.98	30-1.9 (1.97-1.9)	0.316	0.041 (0.066)	35.1 (14.0)	98.3 (86.6)	4.4 (3.1)
100	57.51	150.00	30-1.9 (1.97-1.9)	0.302	0.034 (0.063)	39.9 (16.6)	98.3 (86.7)	4.3 (3.1)
110	57.60	150.08	30-1.9 (1.97-1.9)	0.313	0.030 (0.057)	48.3 (18.4)	98.2 (86.2)	4.4 (3.1)
120	57.66	150.26	30-1.9 (1.97-1.9)	0.325	0.029 (0.055)	48.2 (18.1)	98.3 (86.8)	4.4 (3.1)
130	57.82	150.53	30-1.9 (1.97-1.9)	0.296	0.028 (0.053)	49.4 (19.2)	98.2 (86.2)	4.4 (3.1)
135	57.97	150.75	30-1.9 (1.97-1.9)	0.262	0.026 (0.045)	53.1 (22.9)	98.1 (85.7)	4.4 (3.1)
140	58.08	150.88	30-1.9 (1.97-1.9)	0.323	0.027 (0.046)	50.5 (21.0)	98.1 (85.8)	4.4 (3.1)
145	58.19	150.97	30-1.9 (1.97-1.9)	0.468	0.027 (0.056)	50.2 (18.7)	97.9 (84.7)	4.4 (3.1)
150	58.29	151.02	30-1.9 (1.97-1.9)	0.600	0.030 (0.076)	45.6 (14.6)	98.0 (85.4)	4.4 (3.1)
155	58.38	151.03	30-1.9 (1.97-1.9)	0.722	0.037 (0.104)	37.8 (10.1)	98.0 (85.7)	4.4 (3.1)
160	58.45	151.00	30-1.9 (1.97-1.9)	0.818	0.046 (0.129)	31.0 (7.3)	98.0 (86.2)	4.4 (3.1)

[a] $R_{sym} = \Sigma |I - \langle I \rangle| / \Sigma \langle I \rangle$

Table S8. Refinement statistics of Thau-0.9M

Temp (K)	Unique reflections	R factor [a]	R_{free} factor [b]	B factor (Å^2) – main chain	Self-RMS deviation [c] (Å)	WDD peak position (Å) [d]
80	20343	0.162	0.212	9.05	0	3.09
90	20347	0.163	0.215	9.42	0.045	3.10
100	20390	0.161	0.215	9.55	0.04	3.10
110	20455	0.165	0.219	9.94	0.056	3.11
120	20505	0.161	0.222	10.20	0.064	3.14
130	20646	0.162	0.223	10.05	0.089	3.18
135	20767	0.163	0.216	10.02	0.105	3.26
140	20843	0.160	0.216	10.55	0.122	3.29
145	20922	0.165	0.215	11.82	0.144	3.35
150	21003	0.164	0.226	13.38	0.152	3.42
155	21088	0.169	0.215	14.87	0.166	3.56
160	21150	0.170	0.221	16.43	0.172	3.64

[a] R factor = $\Sigma |F_o| - |F_c| / \Sigma |F_{obs}|$

[b] R_{free} factor is calculated the same as R factor, except it uses 5 % of reflection data omitted from refinement

[c] Self-RMS deviation was calculated between the structure at 80 K and the structures at higher temperatures of Thau-0.9M.

[d] WDD peak position in d-spacing: $d = 2\pi/Q$, where the momentum transfer vector Q is given by $Q = 4\pi\sin(\theta)/\lambda$, where λ is the X-ray wavelength and 2θ is the angle between the incident beam and the diffracted X-rays.

Table S9. Data collection statistics of Thau-control

Temp (K)	Unit-cell dimensions (Å)		Resolution (Å)	Mosaicity (°)	R_{sym} [a]	I/σ(I)	Completeness (%)	Redundancy
	a=b	c						
80	57.76	149.80	30-1.9 (1.97-1.9)	0.377	0.043 (0.071)	30.9 (13.2)	97.0 (92.8)	4.4 (2.8)
90	57.78	149.84	30-1.9 (1.97-1.9)	0.378	0.057 (0.077)	24.8 (11.0)	97.1 (93.2)	4.4 (2.9)
100	57.79	149.88	30-1.9 (1.97-1.9)	0.376	0.044 (0.072)	29.8 (12.8)	97.2 (93.1)	4.5 (2.9)
110	57.80	149.92	30-1.9 (1.97-1.9)	0.376	0.043 (0.070)	30.0 (12.9)	97.3 (93.5)	4.5 (2.9)
120	57.81	149.96	30-1.9 (1.97-1.9)	0.374	0.041 (0.070)	31.0 (13.2)	97.3 (93.4)	4.4 (2.9)
130	57.82	150.00	30-1.9 (1.97-1.9)	0.373	0.041 (0.071)	30.9 (13.0)	97.3 (93.4)	4.4 (2.9)
135	57.83	150.02	30-1.9 (1.97-1.9)	0.375	0.041 (0.070)	30.9 (12.9)	97.3 (93.3)	4.4 (2.9)
140	57.84	150.05	30-1.9 (1.97-1.9)	0.375	0.043 (0.073)	30.3 (12.2)	97.3 (93.1)	4.4 (2.8)
145	57.85	150.08	30-1.9 (1.97-1.9)	0.376	0.042 (0.071)	31.2 (12.9)	97.4 (93.5)	4.4 (2.9)
150	57.87	150.11	30-1.9 (1.97-1.9)	0.378	0.042 (0.071)	31.1 (12.6)	97.4 (93.4)	4.4 (2.9)
155	57.89	150.14	30-1.9 (1.97-1.9)	0.380	0.042 (0.073)	30.8 (12.4)	97.4 (93.6)	4.4 (2.9)
160	57.91	150.19	30-1.9 (1.97-1.9)	0.379	0.042 (0.075)	30.8 (12.0)	97.4 (93.5)	4.4 (2.9)

[a] $R_{sym} = \Sigma |I - \langle I \rangle| / \Sigma \langle I \rangle$

Table S10. Refinement statistics of Thau-control

Temp (K)	Unique reflections	R factor [a]	R_{free} factor [b]	B factor (Å^2) – main chain	Self-RMS deviation [c] (Å)	WDD peak position (Å) [d]
80	20434	0.152	0.201	10.27	0	3.78
90	20231	0.157	0.200	10.35	0.038	3.74
100	20249	0.152	0.202	10.45	0.038	3.73
110	20232	0.152	0.200	10.48	0.037	3.72
120	20310	0.150	0.211	10.55	0.041	3.73
130	20331	0.153	0.192	10.68	0.044	3.73
135	20334	0.152	0.196	10.83	0.044	3.74
140	20549	0.151	0.194	10.97	0.047	3.76
145	20363	0.151	0.193	11.02	0.049	3.74
150	20384	0.152	0.202	11.00	0.052	3.75
155	20394	0.155	0.201	11.22	0.055	3.76
160	20432	0.154	0.197	11.22	0.058	3.77

[a] R factor = $\Sigma |F_o| - |F_c| / \Sigma |F_{obs}|$

[b] R_{free} factor is calculated the same as R factor, except it uses 5 % of reflection data omitted from refinement

[c] Self-RMS deviation was calculated between the structure at 80 K and the structures at higher temperatures of Thau-control.

[d] WDD peak position in d-spacing: $d = 2\pi/Q$, where the momentum transfer vector Q is given by $Q = 4\pi\sin(\theta)/\lambda$, where λ is the X-ray wavelength and 2θ is the angle between the incident beam and the diffracted X-rays.

Table S11. Data collection statistics of Thau-control-noGLY

Temp (K)	Unit-cell dimensions (Å)		Resolution (Å)	Mosaicity (°)	R_{sym} [a]	I/σ(I)	Completeness (%)	Redundancy
	a=b	c						
80	57.58	149.40	50-1.8 (1.83-1.8)	0.654	0.105 (0.339)	15.7 (2.6)	95.0 (97.2)	4.0 (3.5)
90	57.60	149.41	50-1.8 (1.83-1.8)	0.665	0.103 (0.347)	15.3 (2.5)	95.2 (97.2)	4.0 (3.5)
100	57.61	149.46	50-1.8 (1.83-1.8)	0.655	0.105 (0.361)	15.2 (2.3)	95.1 (95.3)	4.0 (3.4)
105	57.63	149.49	50-1.8 (1.83-1.8)	0.659	0.105 (0.360)	15.2 (2.4)	95.0 (96.4)	4.0 (3.5)
110	57.63	149.52	50-1.8 (1.83-1.8)	0.659	0.106 (0.372)	15.0 (2.1)	95.0 (95.3)	4.0 (3.5)
115	57.65	149.56	50-1.8 (1.83-1.8)	0.660	0.105 (0.362)	15.2 (2.4)	95.0 (96.9)	4.0 (3.5)
120	57.67	149.59	50-1.8 (1.83-1.8)	0.661	0.106 (0.402)	14.6 (2.0)	95.0 (95.8)	4.0 (3.4)
125	57.68	149.61	50-1.8 (1.83-1.8)	0.664	0.105 (0.371)	14.8 (2.2)	95.0 (96.9)	4.0 (3.5)
128	57.69	149.64	50-1.8 (1.83-1.8)	0.663	0.105 (0.389)	14.7 (2.1)	95.0 (95.7)	4.0 (3.5)
131	57.70	149.66	50-1.8 (1.83-1.8)	0.667	0.106 (0.402)	14.5 (2.0)	95.0 (95.7)	4.0 (3.5)
135	57.71	149.68	50-1.8 (1.83-1.8)	0.666	0.106 (0.395)	14.4 (1.9)	95.0 (96.0)	4.0 (3.5)
138	57.71	149.69	50-1.8 (1.83-1.8)	0.662	0.106 (0.397)	14.4 (1.9)	95.0 (96.1)	4.0 (3.4)
141	57.72	149.72	50-1.8 (1.83-1.8)	0.660	0.106 (0.390)	14.3 (1.9)	95.0 (96.0)	4.0 (3.4)
145	57.73	149.75	50-1.8 (1.83-1.8)	0.657	0.105 (0.401)	14.1 (1.9)	95.0 (96.0)	4.0 (3.4)
150	57.75	149.80	50-1.8 (1.83-1.8)	0.654	0.105 (0.406)	14.0 (1.9)	95.0 (96.2)	4.0-(3.5)
155	57.78	149.86	50-1.8 (1.83-1.8)	0.643	0.104 (0.400)	14.0 (1.9)	95.1 (96.2)	4.0 (3.5)
160	57.82	149.93	50-1.8 (1.83-1.8)	0.628	0.102 (0.376)	14.1 (2.0)	95.1 (96.7)	4.0 (3.5)

[a] $R_{sym} = \Sigma |I - \langle I \rangle| / \Sigma \langle I \rangle$

Table S12. Refinement statistics of Thau-control-noGLY

Temp (K)	Unique reflections	R factor [a]	R_{free} factor [b]	B factor (Å^2) – main chain	Self-RMS deviation [c] (Å)	WDD peak position (Å) [d]
80	23204	0.169	0.211	17.20	0	n/a
90	23271	0.168	0.206	17.35	0.045	n/a
100	23706	0.169	0.225	17.35	0.048	n/a
105	23246	0.169	0.209	17.45	0.047	n/a
110	23637	0.169	0.215	17.56	0.050	n/a
115	23291	0.170	0.208	17.45	0.052	n/a
120	23729	0.172	0.236	17.53	0.054	n/a
125	23304	0.173	0.220	17.54	0.057	n/a
128	23679	0.168	0.217	17.58	0.056	n/a
131	23672	0.173	0.227	17.52	0.057	n/a
135	23679	0.168	0.226	17.62	0.055	n/a
138	23767	0.168	0.224	17.64	0.063	n/a
141	23779	0.170	0.222	17.37	0.065	n/a
145	23788	0.170	0.223	17.40	0.067	n/a
150	23803	0.168	0.222	17.35	0.067	n/a
155	23824	0.169	0.222	17.13	0.071	n/a
160	23484	0.168	0.207	17.28	0.080	n/a

[a] R factor = $\Sigma\ |F_o| - |F_c| / \Sigma\ |F_{obs}|$

[b] R_{free} factor is calculated the same as R factor, except it uses 5 % of reflection data omitted from refinement

[c] Self-RMS deviation was calculated between the structure at 80 K and the structures at higher temperatures of Thau-control-noGLY.

[d] WDD peak position in d-spacing: $d = 2\pi/Q$, where the momentum transfer vector Q is given by $Q = 4\pi\sin(\theta)/\lambda$, where λ is the X-ray wavelength and 2θ is the angle between the incident beam and the diffracted X-rays.